Journal of Atmospheric and Solar-Terrestrial Physics 73 (2011) 686–702

Contents lists available at ScienceDirect

Journal of Atmospheric and Solar-Terrestrial Physics

journal homepage: www.elsevier.com/locate/jastp

A statistical study of magnetosphere–ionosphere coupling in the Lyon–Fedder–Mobarry global MHD model

B. Zhang [a,*], W. Lotko [a], M.J. Wiltberger [b], O.J. Brambles [a], P.A. Damiano [a]

[a] Thayer School of Engineering, Dartmouth College, Hanover, NH03755, USA
[b] High Altitude Observatory, National Center for Atmospheric Research, Boulder, Colorado, USA

ARTICLE INFO

Article history:
Received 26 May 2010
Received in revised form
20 September 2010
Accepted 22 September 2010
Available online 13 October 2010

Keywords:
Magnetosphere ionosphere coupling
Geospace simulation
Field-aligned current
Ionospheric convection
Field-aligned Poynting flux
Field-aligned vorticity

ABSTRACT

The statistics of magnetosphere–ionosphere (MI) coupling derived from a two-month long run of the Lyon–Fedder–Mobarry (LFM) global simulation model are investigated. MI coupling characteristics such as polar cap potential and field-aligned current (FAC), downward Poynting flux and vorticity of ionospheric convection are compared with observed statistical averages and with results from the Weimer 05 empirical model. The comparisons for eight different IMF clock-angle orientations show that the LFM model produces reasonably accurate average distributions of the Region I and Region II currents. Both current systems have average amplitudes similar to those observed by the Iridium satellite constellation; however, the average LFM amplitudes are smaller by a factor of two compared with the values from the Weimer 05 model. The comparisons of polar cap potential show that the LFM model produces reasonable patterns of ionospheric convection, but the average cross polar cap potential (CPCP) is greater than the observed results by a factor of approximately 2 and greater than Weimer 05 by a factor of 1.5. The differences in convection in LFM results relative to the Weimer 05 model accounts for much of the difference in the Poynting flux patterns and integrated power produced by the two models. The comparisons of average ionospheric field-aligned vorticity show good agreement on the dayside; however, the LFM model gives higher nightside vorticity which may imply that the ionospheric conductance on the nightside is too small in the simulation.

1. Introduction

Among the various approaches to geospace environmental modeling and forecasting, the use of global magnetohydrodynamic (MHD) models is probably the most challenging to implement, but it also holds the greatest promise for accurate specification. One key feature of most global MHD models is the implementation of magnetosphere–ionosphere (MI) coupling, which involves both electrodynamic and plasma transport processes acting between the two regions. The Earth's magnetosphere supplies energy to the ionosphere while the ionosphere dynamically responds by redistributing its plasma and ionization to affect the magnetospheric state (Lotko, 2007). In global MHD models of the solar wind-magnetosphere–ionosphere system, the MI coupling algorithm regulates the boundary condition at the interface between the magnetosphere and ionosphere, through which field-aligned current, particle and electromagnetic energy fluxes flow (Janhunen et al., 1996; Raeder, 2003; Lyon et al., 2004). As a result, ionospheric quantities such as field-aligned current, convection and Poynting flux calculated from a global simulation model are useful variables for evaluating the fidelity of the MI coupling model in a global simulation code.

Most comparisons between global MHD simulations and observations are event studies, in which either global or point measurements are compared with simulation field variables. While such comparisons are useful in validating the model and in providing a global context for the point measurements, we have found that instantaneous results from a simulation can deviate significantly from average statistical behavior. Thus statistical studies provide an alternative means of investigating the fidelity of global MHD simulations of the geospace environment. Data-model comparisons of average states can also yield useful insights into robust features of the model that accurately capture the physics of the actual system or that fail to realistically represent it.

The precedent for the type of study envisioned here was first reported by Guild et al. (2008a,b) who compared statistical properties of the plasma sheet observed by Geotail with LFM simulation results obtained from a two-month long simulation (23 February–26 April 1996) in which WIND satellite observations were used as upstream boundary conditions to drive the Lyon–Fedder–Mobarry (LFM) model. The solar wind and interplanetary magnetic field (IMF) driving conditions and geomagnetic activity during the interval studied by

* Corresponding author.
E-mail addresses: bzhang@dartmouth.edu (B. Zhang), wlotko@dartmouth.edu (W. Lotko), wiltbemj@ucar.edu (M.J. Wiltberger), ojbrambles@dartmouth.edu (O.J. Brambles), pdamiano@dartmouth.edu (P.A. Damiano).

1364-6826/$ - see front matter © 2010 Elsevier Ltd. All rights reserved.
doi:10.1016/j.jastp.2010.09.027

Guild et al. were variable though without extremes, e.g., Dst ≥ -66 nT. This statistical study may be viewed as a subset of a more comprehensive climatology study for the LFM model. It is reasonable to use this kind of "long run" simulation for comparisons between global MHD models and statistical observations. We have analyzed the archived simulation data from Guild et al. (2008a) to produce statistical distributions of high-latitude convection and field-aligned current, vorticity and Poynting flux from the LFM model. Although observational data of these MI coupling variables are not readily available for the two-month simulation interval developed by Guild et al. (2008a), more extensive climatology studies of these variables have been reported.

To study the average field-aligned current system in the LFM model, simulation results may be compared with statistical global field-aligned current distributions derived from 1550 two-hour intervals of magnetic field observations by the Iridium constellation, which are also binned by IMF clock angle and season (Anderson et al., 2008; Green et al., 2009). To evaluate the ionospheric convection patterns in the LFM model, a statistical convection model derived from SuperDARN line-of-sight plasma velocity measurements from 1998 to 2002 can be used for data-model comparison. The observed average convection patterns are also binned by IMF magnitude, clock angle, dipole tilt and season (Pettigrew et al., in press). Field-aligned vorticity is the shear in the ionospheric convection velocity. It is sometimes used as a proxy for ionospheric field-aligned current (given a distribution of ionospheric conductance), and it provides insights into turbulent processes that link the ionosphere and magnetosphere. Therefore, field-aligned vorticity it is another useful point of comparison for MI coupling. Chisham et al. (2009) developed high-latitude distributions of average field-aligned vorticity derived from six-years of SuperDARN measurements in the northern ionosphere, binned by IMF clock angle and season. The distributions and gradients of both ionospheric conductance and field-aligned current constrain the field-aligned vorticity (Sofko et al., 1995), which can be calculated from the measured velocity field alone.

Empirical models are also available for comparison with global simulation results. In particular, the Weimer 05 empirical model (Weimer, 2005) derived from two-years of electric and magnetic field data from the DE-2 satellite has been widely used to produce high-latitude convection and field-aligned current distributions for given upstream conditions. Input parameters to the Weimer 05 model include average solar wind density, speed, IMF magnitude and clock angle, which can be obtained by averaging the upstream boundary condition used in the LFM simulation. Output variables from the Weimer 05 model include high-latitude distributions of ionospheric convection, field-aligned current and Poynting flux, which is essentially equivalent to Joule dissipation rate.

In this paper we report the statistical distributions of field-aligned current, high latitude ionospheric convection pattern, Poynting flux and vorticity derived from the archived two-month LFM simulation data developed in the Guild et al. (2008a) study. These statistical distributions are also compared with the above referenced observational datasets and with results from the Weimer 05 empirical model. Since the simulation time interval was selected near spring equinox, the average dipole tilt angle is small (approximately zero) and the ionospheric conductances of the northern and southern hemispheres are similar; therefore differences in the convection patterns in the northern and southern hemisphere are also small. Only the results in the northern hemisphere are used for data-model comparison.

In Section 2, we briefly describe the existing MI coupling algorithm in the LFM model and the basic information of the "LFM Long Run" simulation data used for analysis. In Section 3, we compare the statistical distributions of ionospheric field-aligned current derived from the LFM simulation with the average maps derived from 1550 two-hour intervals of Iridium constellation magnetometer data and empirical results from the Weimer 05 model. Both IMF clock angle dependence and magnetic local time (MLT) distributions are considered for comparison. We also compare the statistical ionospheric convection patterns in the LFM model with a climatological SuperDARN convection model developed by Pettigrew et al. (in press) and empirical results from the Weimer 05 model. We then compare the statistical field-aligned Poynting flux distributions derived from the LFM model with empirical results obtained from the Weimer 05 model. At the end of Section 3 we analyze the statistical distributions of ionospheric field-aligned vorticity in the LFM simulation and compare the results with SuperDARN measurements in Chisham et al. (2009). In Section 4 we summarize the most important results of our analysis based on the Long Run simulation in the previous sections.

2. Simulation information

2.1. MI coupling in the LFM model

The Lyon–Fedder–Mobarry (LFM) model is a three-dimensional, magnetospheric simulation code that solves ideal MHD equations self-consistently on an irregular, stretched spherical grid. The geomagnetic field is represented in the simulation as a point dipole magnetic field located at the center of the earth. Upstream solar wind conditions obtained from observations are used to drive the simulation at its sunward boundary, corresponding to an SM-coordinate y–z plane located at $x=30\ R_E$. The upstream boundary conditions are taken to be independent of y and z coordinates. In the LFM simulation, the magnetic dipole is at all times is taken to be aligned with the z-direction of the SM coordinate system. Consequently, as the dipole direction rotates about the Earth's spin axis, an appropriate diurnal rocking motion of the upstream solar wind and magnetic field vectors must be introduced in the SM y–z plane to represent the rotation. Details on the grid and numerical techniques in the LFM model are described in Lyon et al. (2004). The LFM code also includes a two-dimensional, electrostatic ionospheric model, which is part of the MI coupling module first presented by Fedder et al. (1995) and Slinker et al. (1999). To facilitate interpretations of the statistical features of MI coupling in the LFM model, basic elements of its MI coupling algorithm are discussed below.

The basic equation of the MI coupling module combines Ohm's law with current continuity and the electrostatic approximation to obtain the following elliptic equation for the ionospheric electric potential Φ_i, given the field-aligned current $J_{\parallel i}$ at the top of the ionospheric conducting layer and the height-integrated conductance tensor $\overline{\overline{\Sigma}}$:

$$\nabla \cdot \overline{\overline{\Sigma}} \cdot \nabla \Phi_i = J_{\parallel i} \cos\alpha. \tag{1}$$

This equation is solved on a two-dimensional, gridded spherical surface. The dip factor $\cos\alpha$ is $\hat{b} \cdot \hat{r}$ where $\hat{b}$ is a unit vector pointing along the dipole magnetic field at the top of the conducting layer and $\hat{r}$ is the spherical polar radial unit vector. In the LFM model, $J_{\parallel i}$ is computed at the low-altitude computational boundary located at 2.2 R_E geocentric in the magnetosphere and is then mapped assuming $J_\parallel/B = \text{const}$ to the top of the ionospheric conducting layer, specified to be 1.02 R_E geocentric, where (1) is solved. The ionospheric electric potential Φ_i is mapped along dipole field lines to the inner computational boundary (2.2 R_E geocentric), and the electric field is calculated as $\mathbf{E} = -\nabla\Phi_i$ which serves as part of the inner boundary condition for the MHD equations. The ionospheric conductance tensor $\overline{\overline{\Sigma}}$ is defined as

$$\overline{\overline{\Sigma}} = \frac{1}{\cos\alpha} \begin{bmatrix} \Sigma_P/\cos\alpha & -\Sigma_H \\ \Sigma_H & \Sigma_P \cos\alpha \end{bmatrix} \tag{2}$$

where Σ_P and Σ_H are the height-integrated Pedersen and Hall conductances. Empirical equations derived by Robinson et al. (1987) are used to modify the spatiotemporal distribution of the auroral contribution to the ionospheric conductance, using electron precipitation properties derived from the LFM precipitation model (Wiltberger et al., 2009). These empirical relations are

$$\Sigma_{P_{Auroral}} = \frac{40\varepsilon}{1+\varepsilon^2} F_{\varepsilon}^{0.5} \tag{3}$$

$$\Sigma_{H_{Auroral}} = 0.45\varepsilon^{0.85}\Sigma_P \tag{4}$$

where ε and F_ε are average energy and energy flux of precipitating electrons. The conductance also includes a contribution from solar EUV ionization, which varies with solar zenith angle and the observed solar radio flux at 10.7 cm. The empirical models for $\Sigma_{P,H_{EUV}}$ are discussed in Wiltberger et al. (2004). The total conductance is

$$\Sigma_{P,H} = \sqrt{\Sigma^2_{P,H_{Auroral}} + \Sigma^2_{P,H_{EUV}}} \tag{5}$$

Since the simulation interval of the LFM Long Run simulation is near spring equinox, the solar EUV contribution to the ionospheric conductances is approximately the same for both northern and southern hemisphere. The simulation results are therefore very similar in both hemispheres.

2.2. The LFM "Long Run" simulation

The LFM Long Run is an archived dataset from an event simulation which spanned two months of universal time, from 02/23/1996 to 04/26/1996. The upstream boundary condition for this simulation was taken from WIND satellite measurements of solar wind density, velocity and temperature and the interplanetary magnetic field (IMF). The observed values were propagated kinetically from the point of observation to the LFM upstream boundary at 30 R_E using the solar wind velocity. The IMF B_x is artificially set to zero at the upstream boundary to insure $\nabla \cdot \mathbf{B} = 0$. The LFM code for this simulation has a grid of $53 \times 48 \times 64$ cells. This event was first used to study plasma sheet climatology by Guild et al. (2008a). The Long Run simulation was implemented by separating the two-month time interval into eight one-week segments, which were run simultaneously on multiple processors to optimize simulation time to solution. For the spatial grid resolution used in this study, it took about one month of computational time for Guild et al. (2008a) to complete the Long Run simulation. The simulation interval chosen for the Long Run study was selected by Guild et al. (2008a) for a somewhat different purpose than in the current study, although this interval serves our purpose in a more limited statistical sense. The distribution of solar wind conditions during the time interval of the simulation were identified as being statistically similar to those during a comparison interval of Geotail plasmasheet observations.

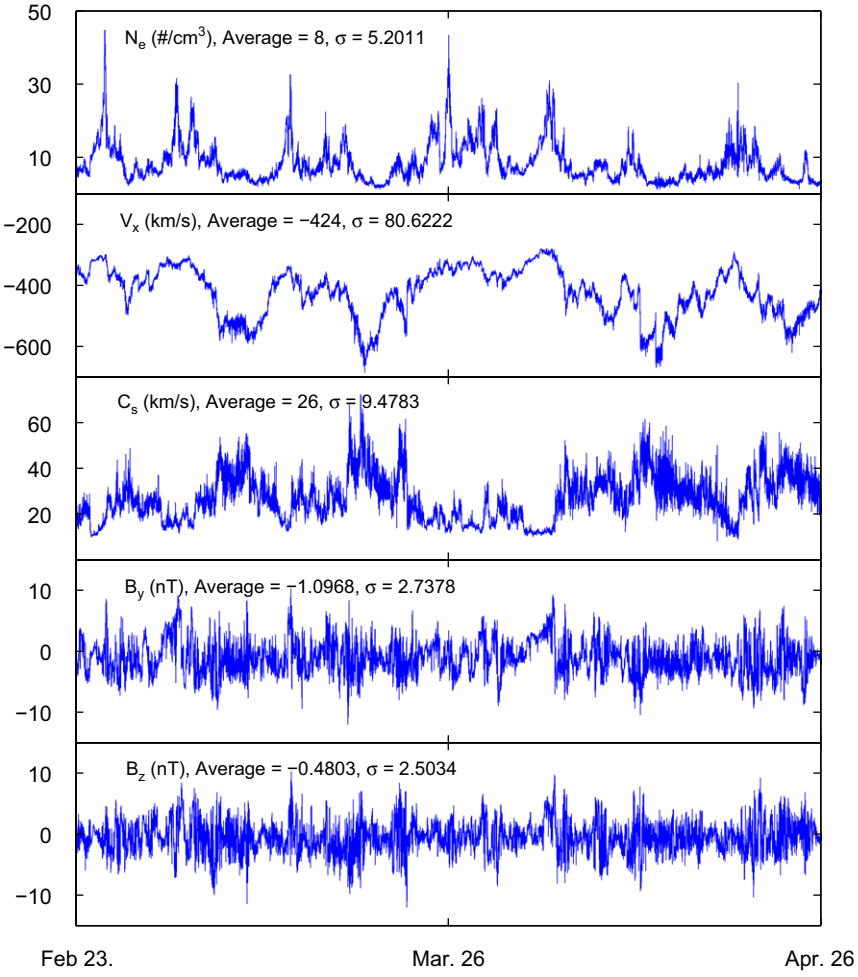

Fig. 1. Solar Wind data used in the Long Run simulation. The average numbers are shown in each panel.

Fig. 1 shows the solar wind data of the selected time interval used in the simulation. The time interval was relatively quiet because no strong perturbations were observed and no major magnetic storms were reported during this two-month period in which Dst ≥ -66 nT. Therefore, this particular event simulation represents only a limited sample of what might be a more comprehensive climatology study.

The average values of the IMF conditions in the Long Run simulation, binned by average clock angle, are shown in Fig. 2. The 0° clock angle bin includes all intervals with IMF orientations between $-22.5°$ and $+22.5°$, and similarly for the other bins. The number of samples in each IMF clock angle bin is shown in Fig. 3, which shows that in this selected time interval, IMF samples within the 225° clock angle bin are most prominent.

3. Results and discussions

3.1. Ionospheric field-aligned currents

Iijima and Potemra (1976a) introduced the concept of Region I and Region II currents as permanent features of the ionospheric current system. The statistical distribution of the ionospheric field-aligned current system in the LFM model can be calculated by

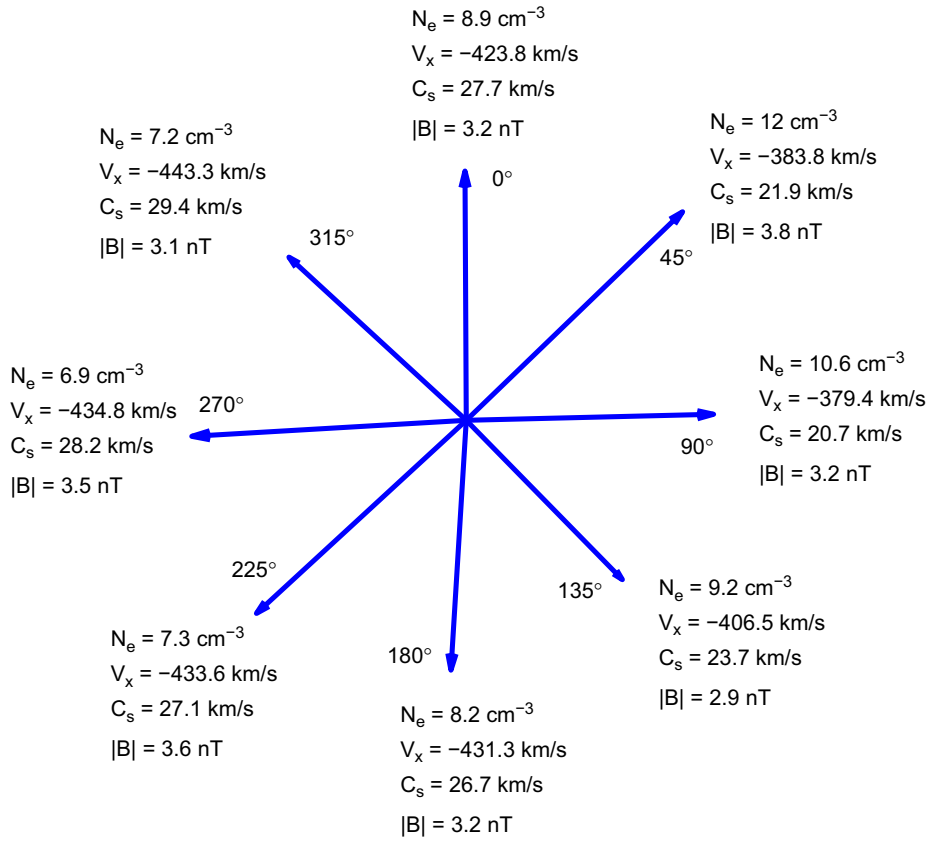

Fig. 2. Average values of solar wind and IMF conditions binned by IMF clock angle. The arrows are the average orientation of IMF in each clock angle bin, together with IMF magnitude, solar wind number density, velocity and sound speed.

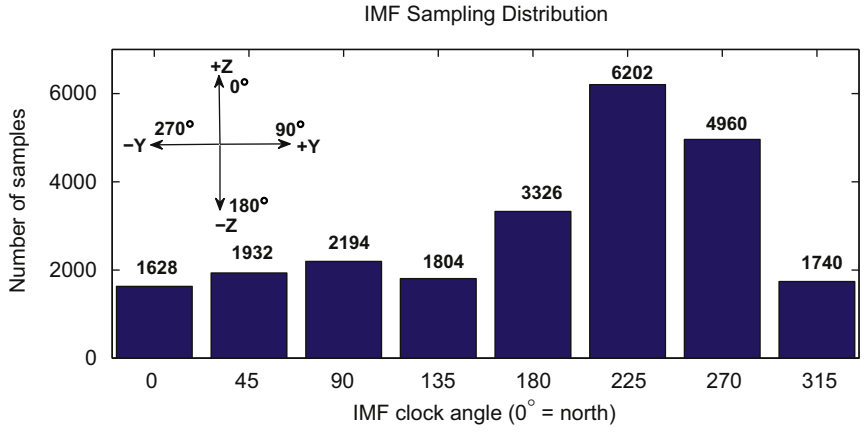

Fig. 3. Number of simulation samples in each IMF clock angle bin, zero degree means the northward IMF bin, which considers IMF samples with clock angle between $-22.5°$ and $22.5°$.

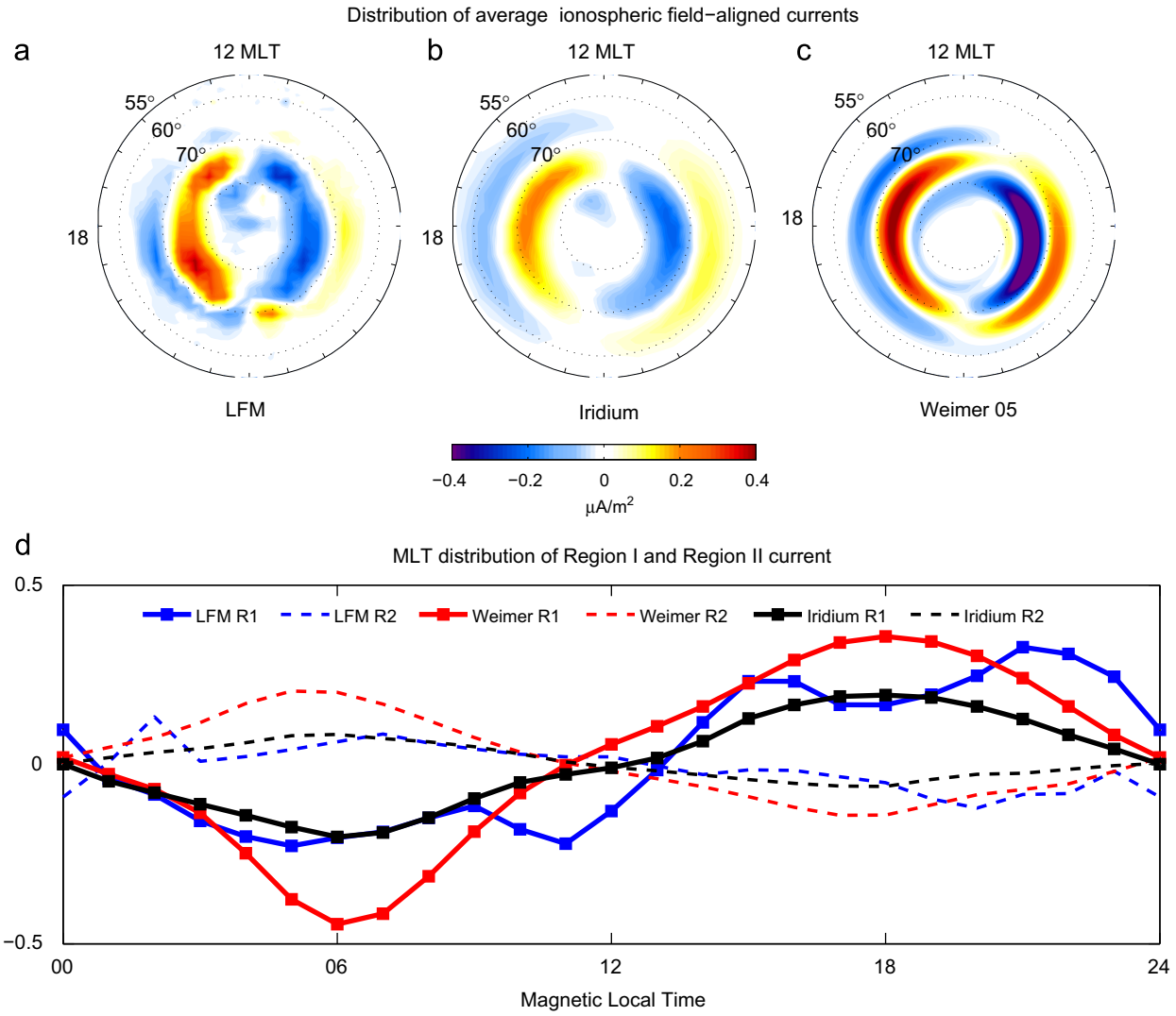

Fig. 4. Average distribution of ionospheric field-aligned current derived from the (a) LFM Long Run simulation; (b) Iridium constellation magnetic field data; (c) Weimer 05 empirical model. (d) Magnetic local time distribution of average Region I and Region II currents calculated from the LFM simulation, Iridium data and Weimer 05 model.

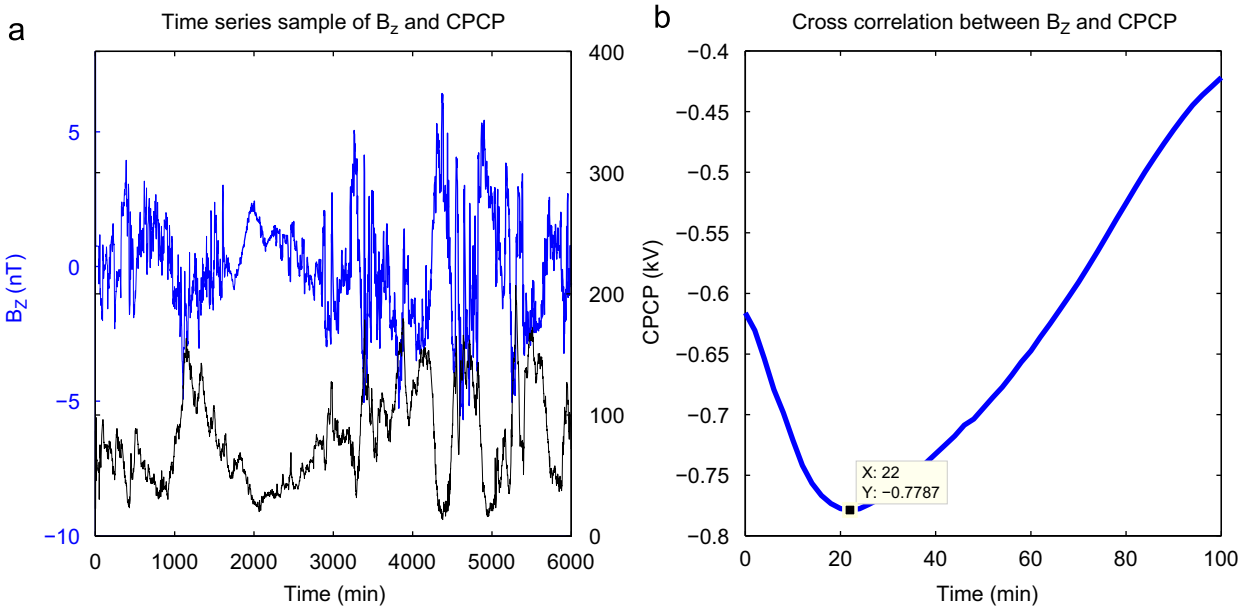

Fig. 5. (a) The time series of B_z and CPCP for cross-correlation analysis. (b) The cross-correlation function for the selected B_z and CPCP series.

averaging the Long Run results over the whole simulation time interval. Fig. 4a shows the average ionospheric field-aligned current distribution for the Long Run. Statistically, two primary ionospheric current systems are evident in the LFM simulation under the weakly disturbed solar wind and IMF conditions of the Long Run: (1) The average Region I current system is located between 70 and 80° latitude, and flows into the ionosphere on the dawnside with average peak values of about 0.5 $\mu A/m^2$ near 0500 and 1100 MLT. The Region I current flowing outward from the duskside ionosphere has peak averages of about $-0.5\,\mu A/m^2$ near 1500 and 2100 MLT. (2) The average Region II current system is located mostly between approximately 65−70° latitude, and is lower in magnitude compared with the Region I current system. The average duskside Region II current flows into the ionosphere with average peak values around 0.26 $\mu A/m^2$, and the dawnside Region II current flows in the opposite direction with peak averages around $-0.25\,\mu A/m^2$. A third current system, or perhaps an extension of the Region I current system, flows into the ionosphere inside 80° latitude in Fig. 4a, with peak averages about $-0.3\,\mu A/m^2$. In observations, these field-aligned currents are sometimes called Region 0 currents (Iijima and Potemra, 1976b) and they are inward (rather than outward) in the Long Run simulation because the IMF distribution shown in Fig. 2 includes more samples with IMF $B_y < 0$ than with $B_y > 0$. Observations and the results to be discussed below show that the Region 0 current system has the polarity in Fig. 4a when IMF $B_y < 0$. Thus the aggregate statistical averages of Fig. 4a give more weight to IMF $B_y < 0$ conditions.

The statistical large-scale distribution of ionospheric currents derived from the Iridium magnetometer data is shown in Fig. 4b.

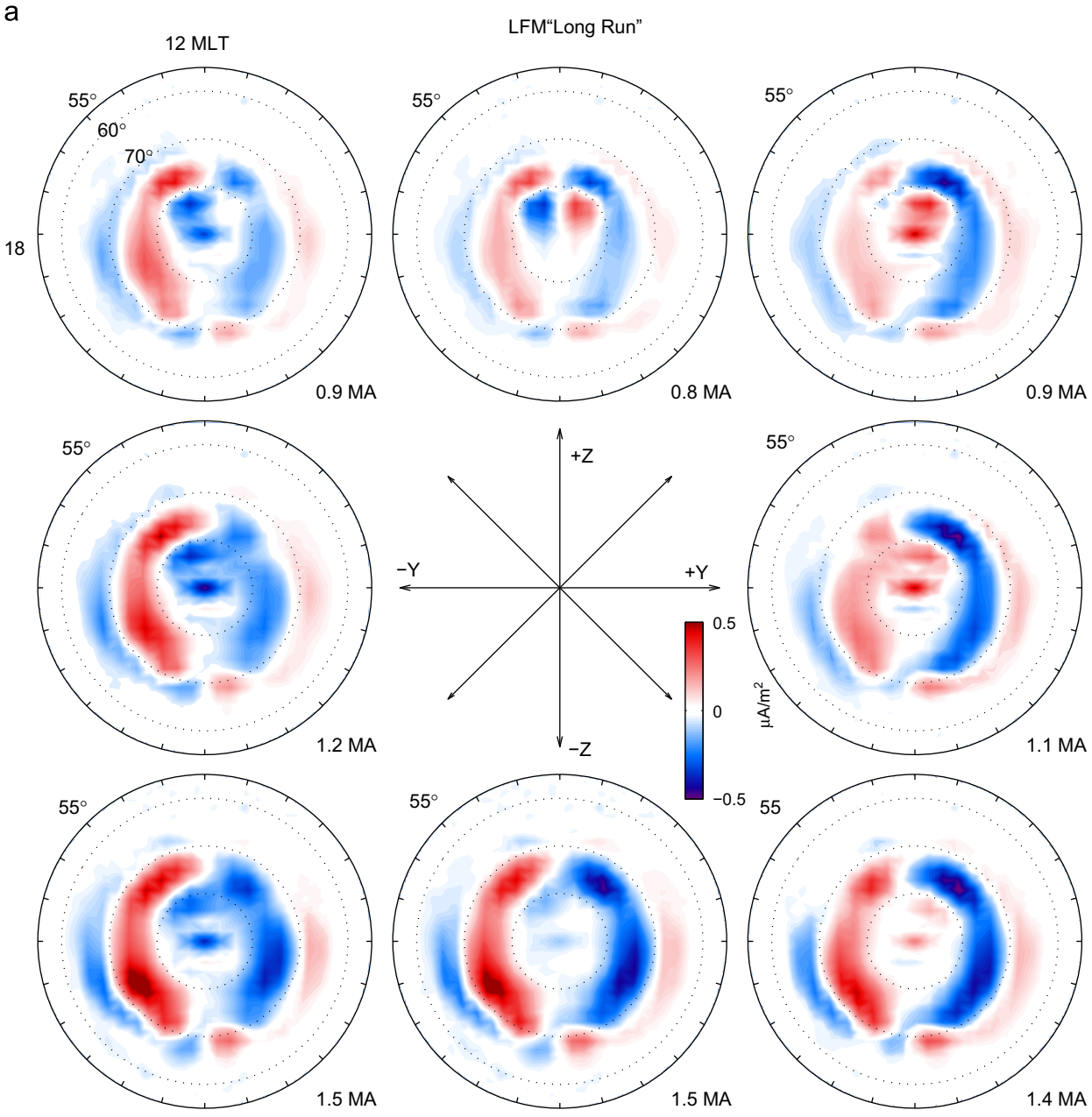

Fig. 6. Statistical distributions of ionospheric field-aligned current obtained from (a) the LFM Long Run simulation and (b) Iridium observations from Anderson et al. (2008), binned by IMF clock angle. The IMF orientation projected in the *Y–Z* GSM plane for each IMF clock angle bin is indicated by the arrows in center panel. The total current flowing into the ionosphere is given in the lower right of each panel.

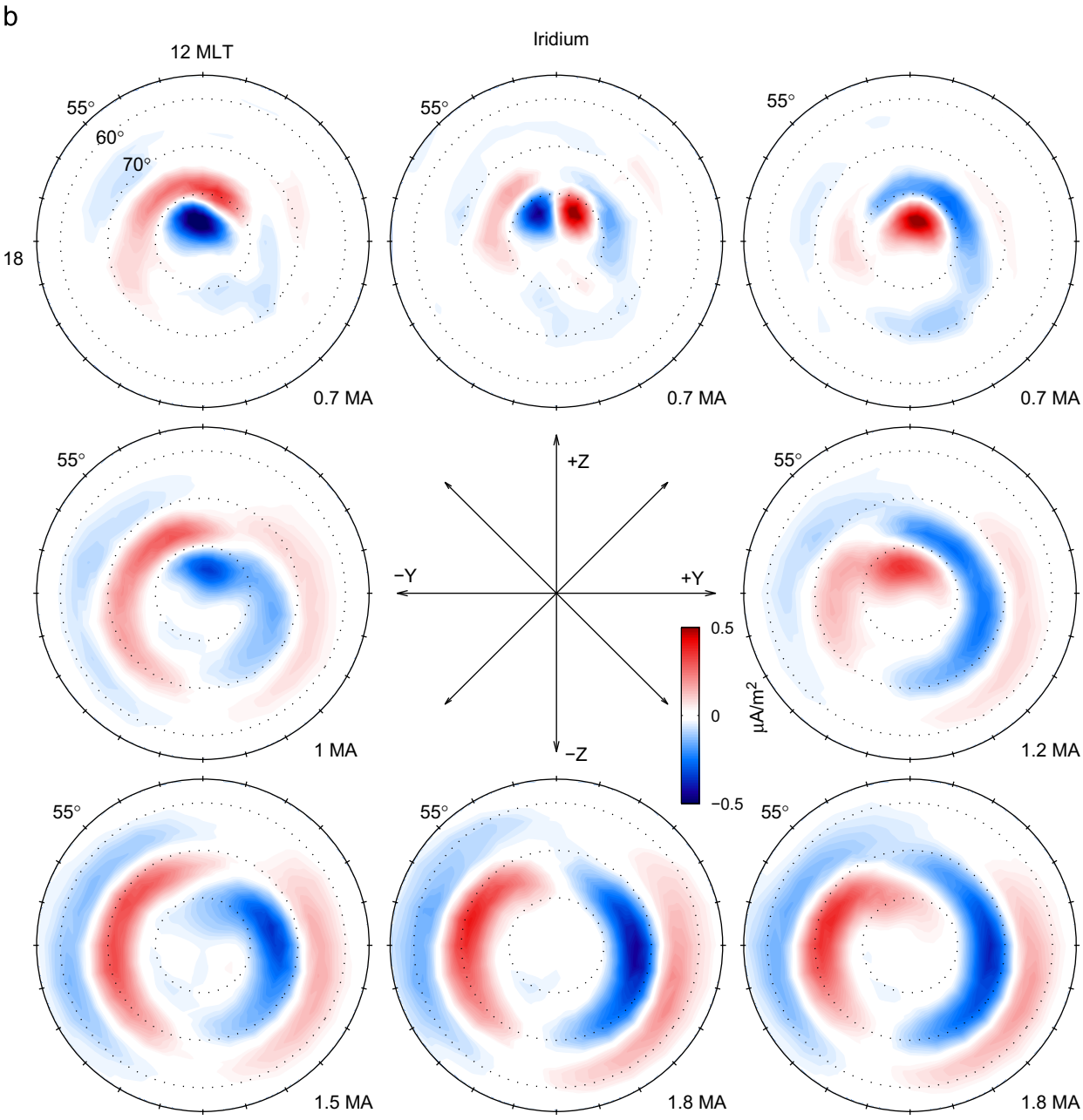

Fig. 6. (*Continued*)

This dataset includes 1550 samples of relatively steady interplanetary conditions over a two-hour interval. The current distribution shown for Iridium in Fig. 4b is calculated as a weighted average of the current distributions in Anderson et al. (2008). The weights are determined by the number of IMF samples in each IMF clock angle bin, shown in Fig. 3. This statistical current distribution is restricted to intervals with stable currents. Therefore, this current distribution is representative of weakly perturbed IMF conditions (though not necessarily quiet conditions) which is similar to the weakly perturbed IMF conditions in the LFM Long Run simulation. From the Iridium magnetometer data, the average Region I current system is located between 70 and 80° latitude while the Region II current system is located between 60 and 70° latitude. The Iridium Region II current distribution is broader in latitude than that in the LFM simulation. The peak value for Region I and Region II currents are ± 0.3 and $\pm 0.15\,\mu A/m^2$, respectively. Due to the influence of IMF B_y, weak currents flow into the ionosphere inside 80° latitude in the Iridium distributions. A similar behavior is observed in the simulation results.

Fig. 4c shows the empirical current system calculated from the Weimer 05 model. This current distribution is calculated by the same weighted average of eight clock-angle binned current distributions from the Weimer 05 model. In the Weimer 05 model, the Region I current system is located between 70 and 80° latitude, and the Region II current system is located between 65 and 70° latitude. The magnitudes of average Region I and Region II currents from the Weimer 05 model are greater than for both LFM simulation and Iridium measurements. The Weimer 05 model is derived from statistical analysis of instantaneous measurements on single-satellite passes, while the Iridium global measurements only include magnetometer data samples when the IMF exhibits weak variability over a two-hour interval. Therefore it is not surprise that the magnitudes of Iridium

current distributions are smaller than Weimer 05 model. This comparison suggests that the magnitude of average ionospheric field-aligned current in the LFM model might be too small.

Fig. 4d shows the magnetic local time distribution of average Region I currents (between 72 and 78° latitude) and Region II currents (between 64 and 70° latitude) calculated from the LFM simulation, the Iridium data and the Weimer 05 empirical model. The MLT distribution of field-aligned current intensity in the LFM simulation varies in a slightly different way compared with both Iridium and Weimer 05 results. According to Iijima and Potemra (1976a), the average Region I current system peaks at 1000 MLT in the morning sector for inward flowing current and 1400 MLT in the afternoon sector for outward flowing current. The MLT distribution of average Region I current from the LFM simulation peaks around 1100 and 1500 MLT on the dayside and 0500 and 2100 MLT on the nightside. The average Region I currents in both Iridium observational and Weimer 05 empirical results have peak values around 0700 and 1700 MLT. The intensity of average Region I current from the LFM simulation is close to that derived from the Iridium measurements and smaller than Weimer 05 empirical results by a factor of 0.4.

Statistically, LFM has a reasonable Region II current system as shown in Fig. 4, which is somewhat unexpected due to the absence of drift-kinetic ring current physics in global MHD models. The Region II currents in the LFM model mainly originate from divergence of an MHD diamagnetic ring current (Wolf et al., 2007). In the LFM simulation, plasma accumulates in the slow flow region of the inner magnetosphere through convection from the tail to the nightside inner magnetosphere. The associated density accumulation and adiabatic compression of the fluid enhances the

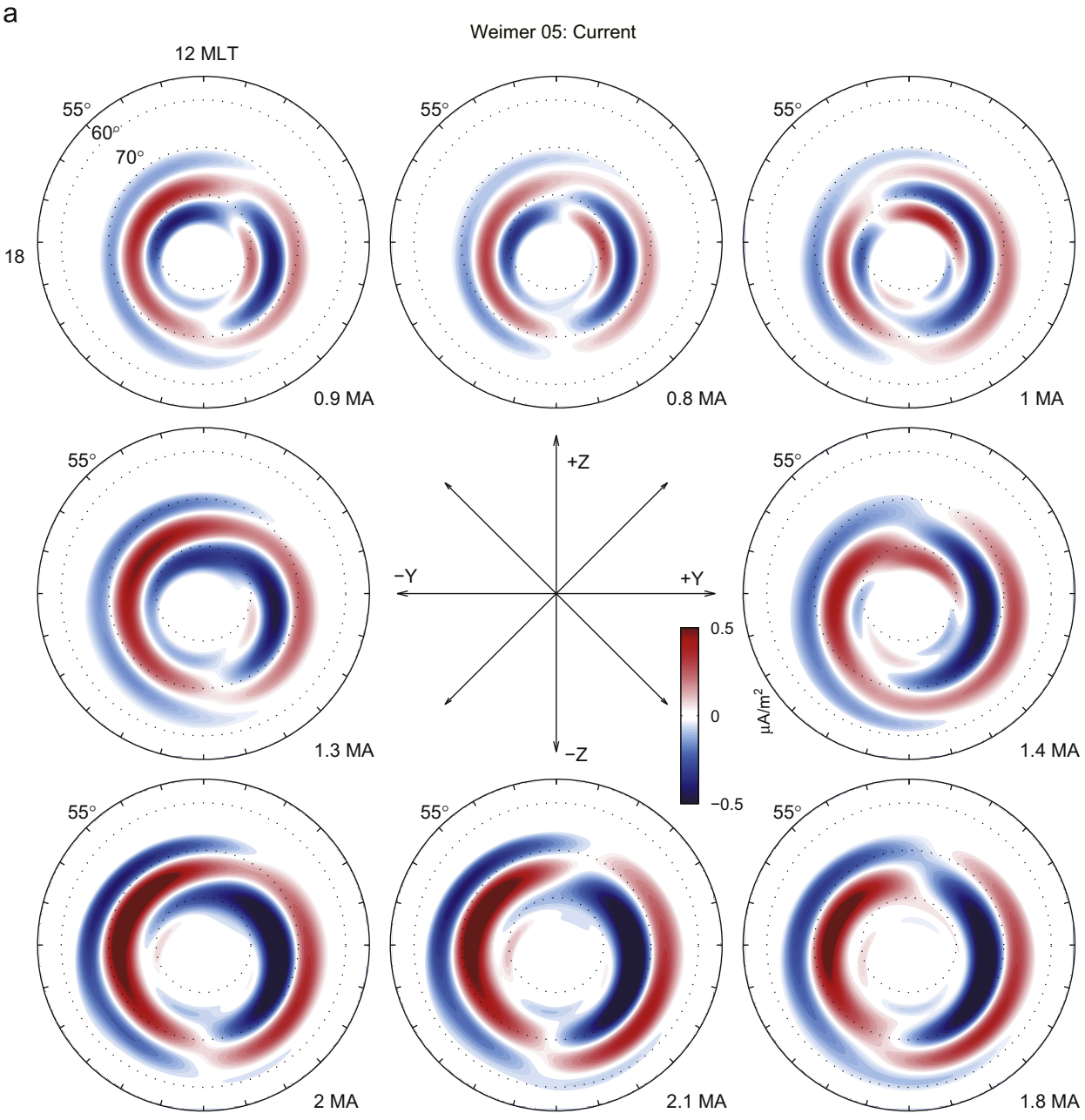

Fig. 7. Empirical distributions of (a) ionospheric field-aligned currents and (b) convection patterns obtained from the Weimer 05 model, binned by IMF clock angle. The inputs to the Weimer 05 model are the average solar wind and IMF conditions shown in Fig. 2. The IMF clock angle for each panel is indicated in the center panel. The total inward current and the cross polar cap potential are shown in the lower right of each panel.

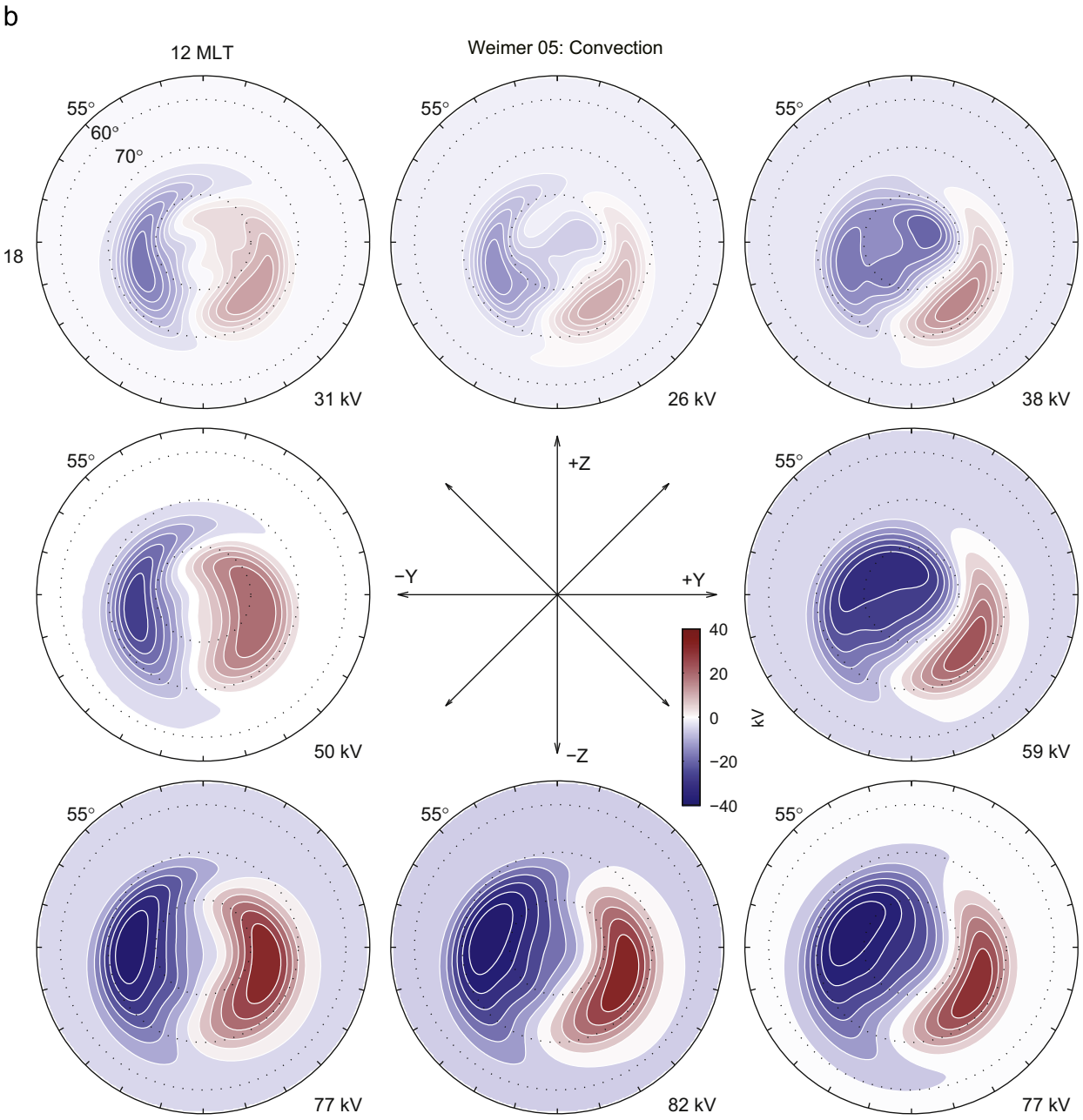

Fig. 7. (*Continued*)

radial pressure gradient that produces the diamagnetic ring current. Azimuthal gradients in the pressure distribution give rise to the Region II currents in the LFM simulation.

To analyze the clock-angle distribution of the simulation data, the ionospheric response should be lagged in time because the response of the magnetosphere–ionosphere system to given upstream conditions is delayed due to the propagation of the solar wind and IMF conditions from the upstream boundary (30 R_E sunward from the Earth). Due to the slow variation of the solar wind and IMF data, we chose a constant average lag time based on a cross-correlation analysis between IMF B_z and the cross polar cap potential (CPCP). Fig. 5a shows samples of B_z and CPCP time series used in the cross-correlation analysis. Fig. 5b shows the cross-correlation function between B_z and CPCP. The cross-correlation function peaks around 22 min. This correlation time is expected for a solar wind propagating from the upstream boundary to the magnetopause with speed around 400 km/s. As a working approximation, 22 min is chosen to be the lag time in subsequent analysis of the IMF clock-angle dependence.

Fig. 6a shows the average distributions of the ionospheric field-aligned current calculated from the LFM simulation binned by the IMF clock angles indicated in the center panel. The SM axis $+Z$ and $+Y$ correspond to northward and eastward IMF at the subsolar dayside magnetopause, respectively. In the LFM simulation, the variations of the average ionospheric field-aligned current distribution are well ordered by IMF clock angle. For southward IMF ($B_z < 0$), the LFM current distributions resemble the statistical results of Iijima and Potemra (1976a). Region I currents are flowing downward (upward) on the dawnside (duskside), with the opposite for Region II currents. Southward IMF also corresponds to a total downward flowing current of 1.5 MA, approximately a factor of 1.8 greater than the value of 0.8 MA for northward IMF.

The average current topology evolves progressively as the IMF clock angle rotates away from southward with the influence of the B_y components, with the basic topology of the average current distribution preserved while the total current flowing into the ionosphere decreases. In addition, the most poleward Region I currents are upward (downward) for IMF $B_y > 0$ ($B_y < 0$). For northward IMF, the NBZ currents near the geomagnetic pole (Iijima et al., 1984) are prominent and both Region I and Region II currents have similar topology to that when IMF $B_z < 0$, but their magnitudes are weaker and they occur at higher latitudes. When the IMF has a $B_y < 0$ component, the total current flowing through the ionosphere is greater than for $B_y > 0$ cases. This asymmetry originates from the asymmetry in the driving solar wind and IMF conditions, evident in Fig. 2, i.e., both the average $|B|$ and average v_{sw} are larger in the two month time series when $B_y < 0$ than when $B_y > 0$.

Fig. 6b shows the IMF clock-angle binned, statistical global field-aligned current distributions derived from 1550 two-hour intervals of the Iridium magnetometer data when the interplanetary conditions were stable (Anderson et al., 2008). The relationship between the IMF clock angle and average field-aligned current distribution in the Iridium results is similar to that in LFM. However, the average total current flowing through the ionosphere is greater in the Iridium sample than in the LFM simulation for the two distributions with IMF clock angle $\theta = 135^\circ$ and 180°. Since the IMF conditions in the LFM Long Run simulation are probably not statistically the same as those for the Iridium samples, such differences are not surprising.

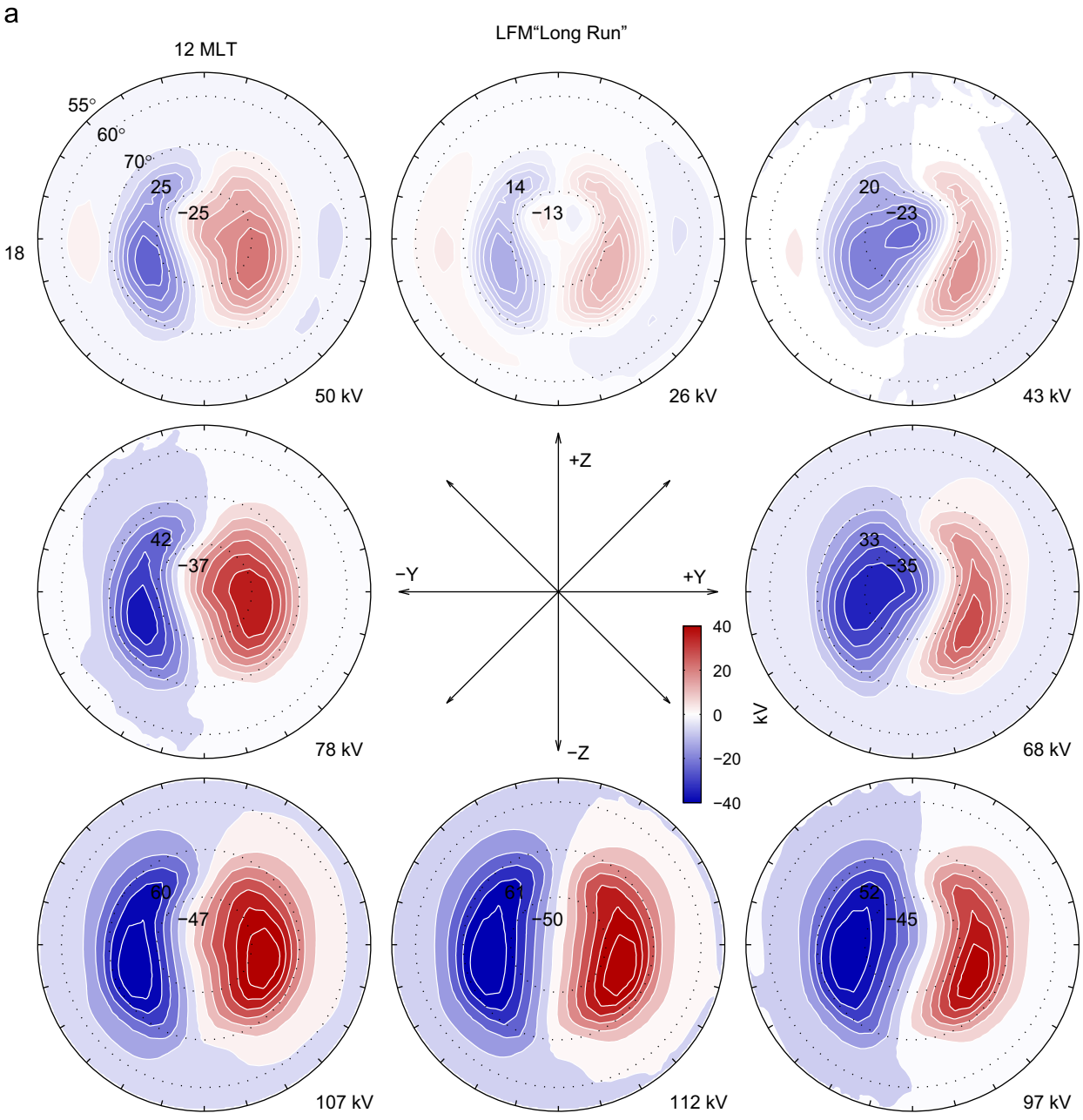

Fig. 8. Statistical distributions of ionospheric convection patterns obtained from (a) the LFM "Long Run" simulation and (b) SuperDARN observations from Pettigrew et al. (in press), binned by IMF clock angle. The IMF orientation for each IMF clock angle bin is indicated in the arrows in center panel. The cross polar cap potential is given in the lower right of each panel.

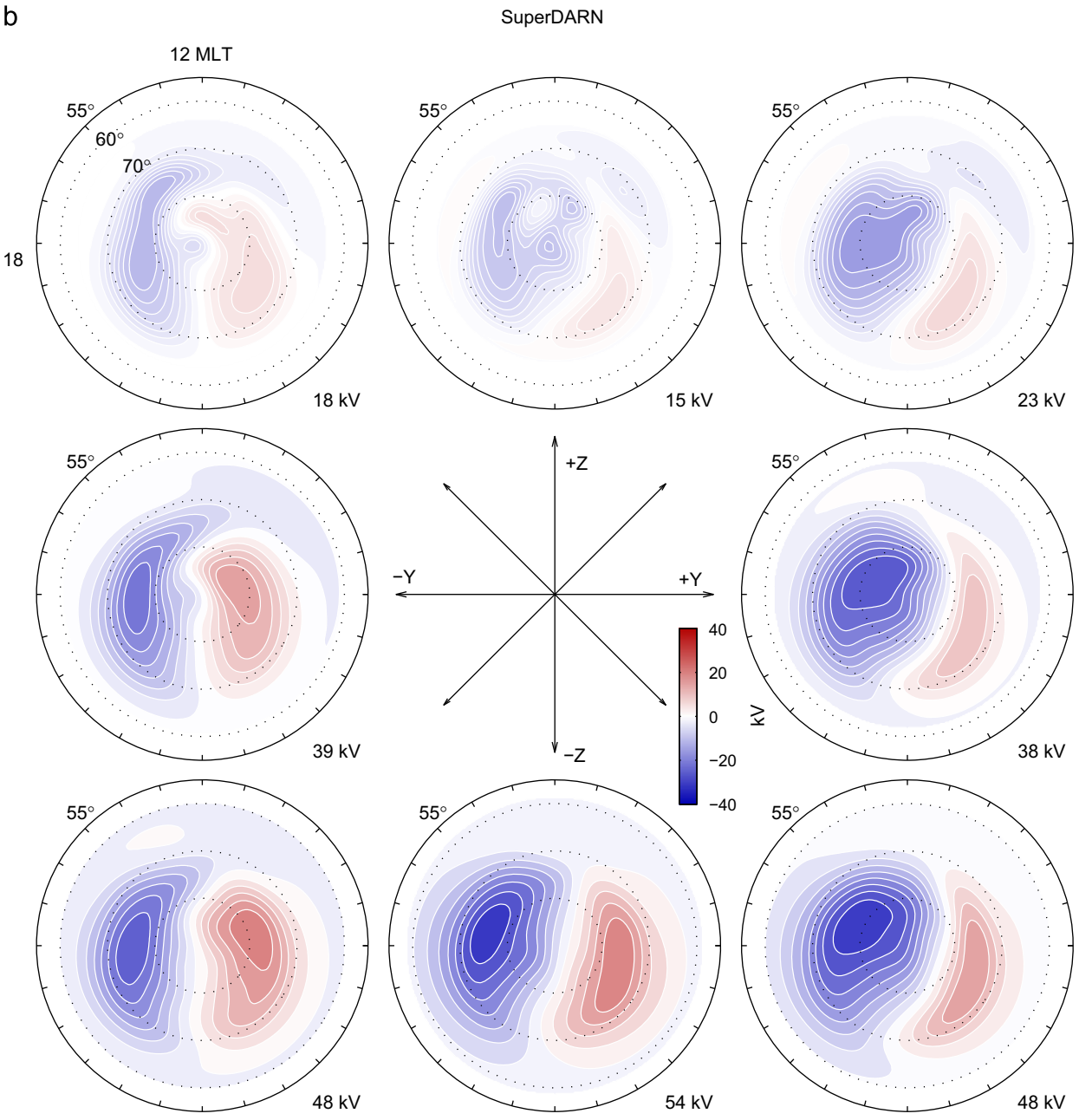

Fig. 8. (*Continued*)

Fig. 7a shows the empirical field-aligned current distributions obtained from the Weimer 05 model. The inputs to the Weimer 05 model are IMF clock angle, average magnitude of solar wind speed and density within each clock angle bin, together with a specific date to set the dipole tilt angle (03/22/1996 for spring equinox, approximately zero average tilt angle). The results from the Weimer 05 model also show a similar evolution of average field-aligned current distribution as the IMF clock angle rotates. However, the average field-aligned current patterns are quite regular owing to the spherical harmonic fit procedure in the empirical model. Also, the Weimer 05 model gives greater average field-aligned current densities. Quantitatively, when IMF $B_z > 0$, the difference between the integrated field-aligned currents in the LFM and Weimer 05 models is relatively small (deviation less than 15%). However, when $B_z < 0$, the average field-aligned current density increases more in the Weimer 05 model than that in the LFM simulation. For the $B_z < 0$ case, the average total current calculated from the LFM simulation is approximately 70% of the Weimer 05 model.

3.2. Ionospheric convection patterns

The average ionospheric convection patterns can be calculated by averaging the ionospheric electric potential Φ_i from the Long Run simulation within each IMF clock angle bin. Fig. 8a shows the average convection patterns in the northern hemisphere derived from the simulation. A basic two-cell convection pattern is evident for all IMF clock angles. As the IMF clock angle increases from northward ($B_z > 0$) to southward ($B_z < 0$), the electric potential (convection strength) increases. The average cross polar cap potential (CPCP) is 26 kV for northward IMF and 112 kV for southward IMF. As the IMF clock angle rotates from $B_y = 0$ to

pure $B_y > 0$ ($B_y < 0$), the two-cell convection patterns are shaped into asymmetric dawn (dusk) cells. For $B_y > 0$ ($B_y < 0$), the dusk convection cell becomes a little more round (crescent-shaped) compared with the dawn convection cell. The average CPCP values for IMF with $B_y < 0$ are greater than those with a $B_y > 0$, which is expected from the statistics of the IMF conditions for this selected two-month time interval, wherein $|B_y|$ is larger for $B_y < 0$ samples than for $B_y > 0$ samples.

Fig. 8b shows statistical ionospheric convection patterns derived from five years (1998–2002 inclusive) of SuperDARN data with IMF conditions 3 nT $< |B| <$ 5 nT, binned by IMF clock angle (Pettigrew et al., in press). The convection patterns derived from the LFM simulation are similar to the global distributions from the SuperDARN observations. The LFM results also evolve in the same way as SuperDARN convection patterns as the IMF clock angle rotates. However, the CPCP values calculated from the LFM simulation are greater than SuperDARN results by a factor of about 2 for each IMF clock angle. Two possible reasons may explain this disagreement. First, the reconnection potential in the MHD simulation maybe too high, thereby resulting in a greater CPCP. Second, the IMF and solar wind conditions in the two-month Long Run simulation is not statistically sufficiently similar to those in the SuperDARN data.

Fig. 7b shows the empirical distributions of the ionospheric convection pattern obtained from the Weimer 05 model. The inputs to the Weimer 05 model are the same as given in Section 3.1. The Weimer 05 model also exhibits two-cell convection patterns that vary in the same way as the LFM and SuperDARN results as the IMF clock angle rotates. Both the Weimer 05 model and SuperDARN observations show significant dawn–dusk asymmetry of convection cells for $B_y \neq 0$, while the average convection patterns in the LFM model are more symmetric. This difference is due in part the lack of a corotating inner

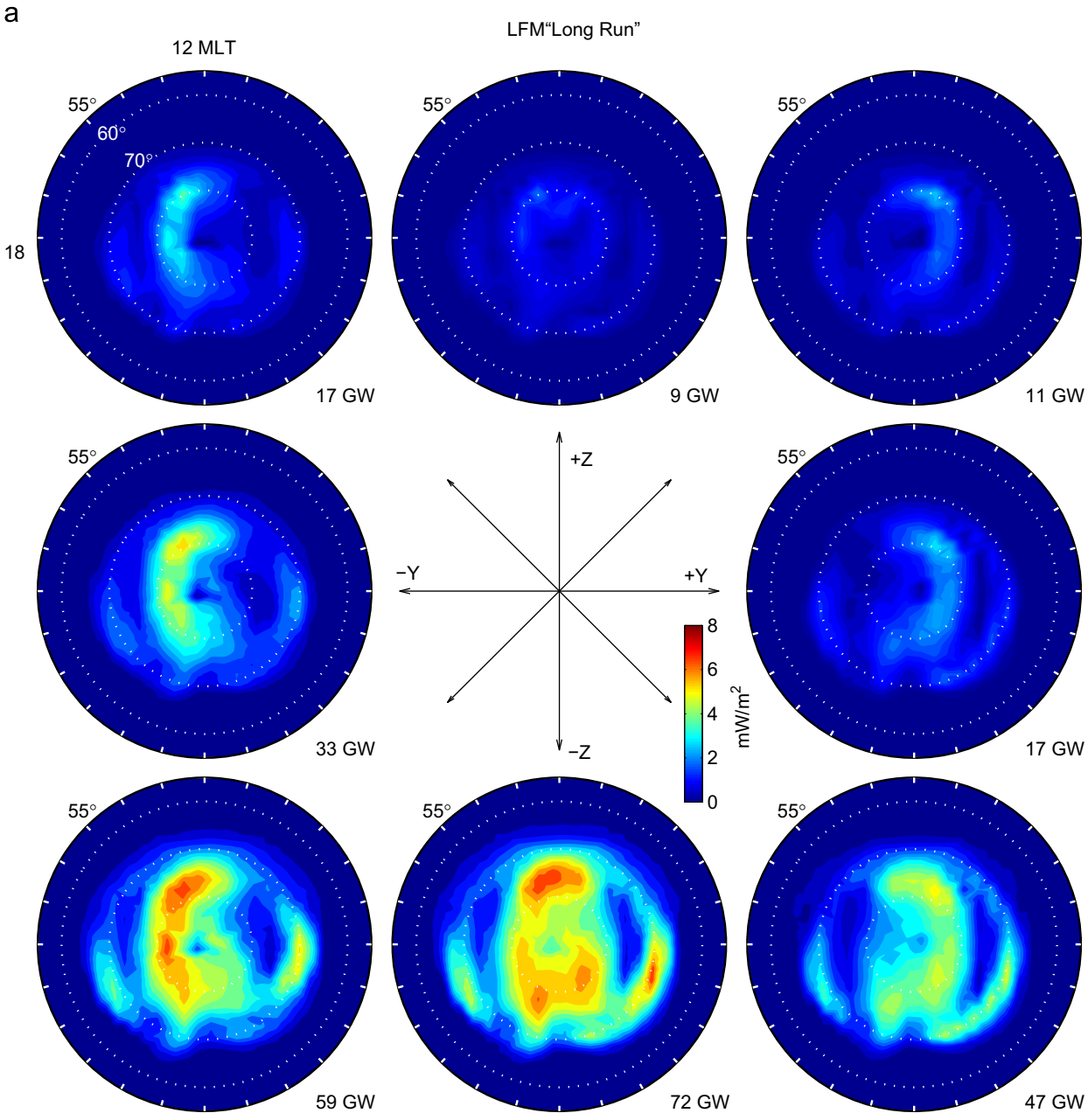

Fig. 9. Statistical distributions of ionospheric Poynting flux obtained from (a) the LFM Long Run simulation and (b) Weimer 05 empirical model, binned by IMF clock angle. The total power flowing into the ionosphere is given in the lower right of each panel.

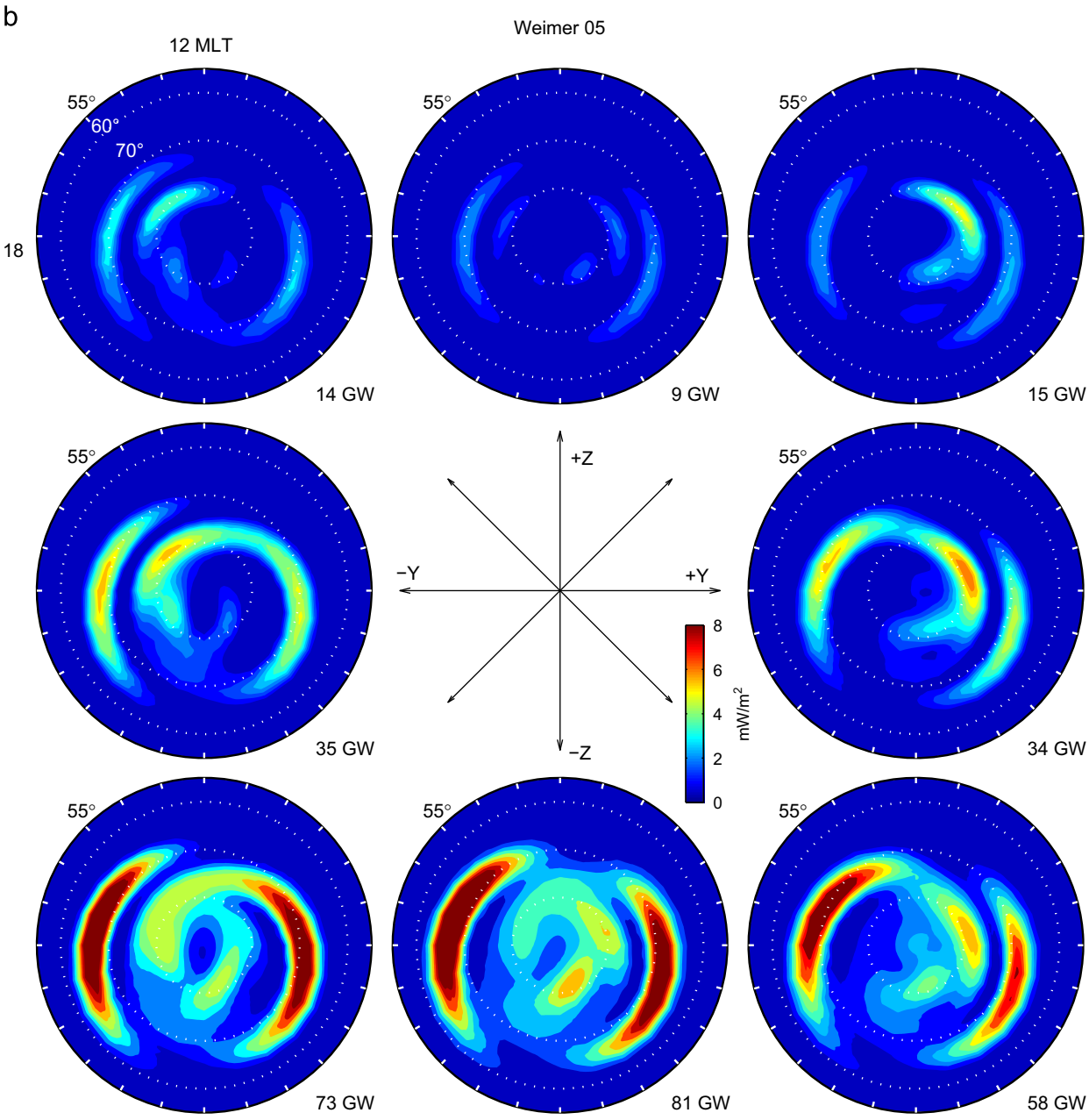

Fig. 9. (*Continued*)

magnetosphere in the LFM simulation. Compared with the empirical results derived from the Weimer 05 model, the CPCP values derived from the LFM simulation are approximately greater by a factor of 1.5.

3.3. Ionospheric Poynting flux

The distribution of Poynting flux is another important feature of MI coupling because it depends on the electrodynamics of the MI interaction. Fig. 9a shows the average downward field-aligned Poynting flux in the Long Run for each IMF clock angle bin. The parallel Poynting flux $S_\parallel$ is calculated at the inner magnetospheric boundary (2.2 R_E geocentric) as

$$S_\parallel = \frac{1}{\mu_0}(\mathbf{E}\times\mathbf{B})\cdot\hat{\mathbf{b}} \tag{6}$$

where $\mathbf{E}$ and $\mathbf{B}$ are the instantaneous electric field and magnetic field taken from the inner boundary, and $\hat{\mathbf{b}}$ is the unit vector pointing along dipole magnetic field lines. $S_\parallel$ is mapped to the ionosphere assuming $S_\parallel/B = \text{const}$. Fig. 9b shows the corresponding distributions of average downward field-aligned Poynting flux obtained from the Weimer 05 empirical model, derived from the vector product of the average electric field and the average magnetic field given by the model. In the LFM simulation, when IMF clock angle rotates from northward to southward, the average total downward flowing power increases by a factor of 8, from 9 to 72 GW. The empirical results from the Weimer 05 model exhibit a similar relationship between IMF clock angle and Poynting flux patterns, i.e., 9 GW for northward IMF and 81 GW for southward IMF. However, in the LFM simulation, downward field-aligned Poynting flux is much more prominent in the high-latitude polar region (inside 75° latitude) than in the Weimer 05

patterns. This result shows that most of the Region I currents close through this region of the ionosphere in the LFM simulation, with less Region I current closing with Region II currents at lower latitudes. In contrast, in the Weimer 05 empirical model, the Poynting flux maximizes in the ionospheric regions where Region I currents close into Region II currents. One possible reason for this disagreement is that in the LFM simulation, the ionospheric conductance is too low in the polar region, which permits a larger electric field there for a given current, a larger Joule dissipation $\mathbf{J}\cdot\mathbf{E}$ and, therefore, a need for higher Poynting flux $S_\parallel$ to power the Joule dissipation.

3.4. Ionospheric field-aligned vorticity

The field-aligned vorticity in the ionosphere is closely linked to both the ionospheric Pedersen conductance and the field-aligned current flowing into and out of the ionosphere. The ionospheric field-aligned vorticity is defined as

$$\Omega_\parallel = (\nabla\times\mathbf{v})\cdot\hat{\mathbf{b}} = \nabla\times\left(\frac{\mathbf{E}\times\mathbf{B}}{B^2}\right)\cdot\hat{\mathbf{b}} \tag{7}$$

where $\mathbf{E}$ is the electric field, $\mathbf{B}$ is the total magnetic field and $\mathbf{v}$ is the plasma velocity in the ionosphere. If we may assume the spatial variation of ionospheric conductance is small compared to the spatial variation of the electric field, then the field-aligned vorticity can be expressed as (Chisham et al., 2009)

$$\Omega_\parallel \approx \frac{\mp J_\parallel}{\Sigma_P B} \tag{8}$$

where the $\mp$ is used in the northern/southern ionosphere. Eq. (8) shows that in regions where the conductance is relatively uniform, e.g., the sunlit ionosphere, the field-aligned vorticity provides an alternative measurement of the ionospheric field-aligned current. In regions where the conductance is more variable, the vorticity provides another point of comparison for validating MI coupling in the LFM model.

The ionospheric electric field $\mathbf{E}$ derived from the LFM model at high latitudes can be used to calculate the ionospheric field-aligned vorticity based on Eq. (7). To good approximation, the magnetic field $\mathbf{B}$ may be taken to be a dipole field. The average field-aligned vorticity distributions derived by Chisham et al. (2009) can be used for data-model comparison. These statistical distributions of ionospheric vorticity are calculated from six-years (2000–2005

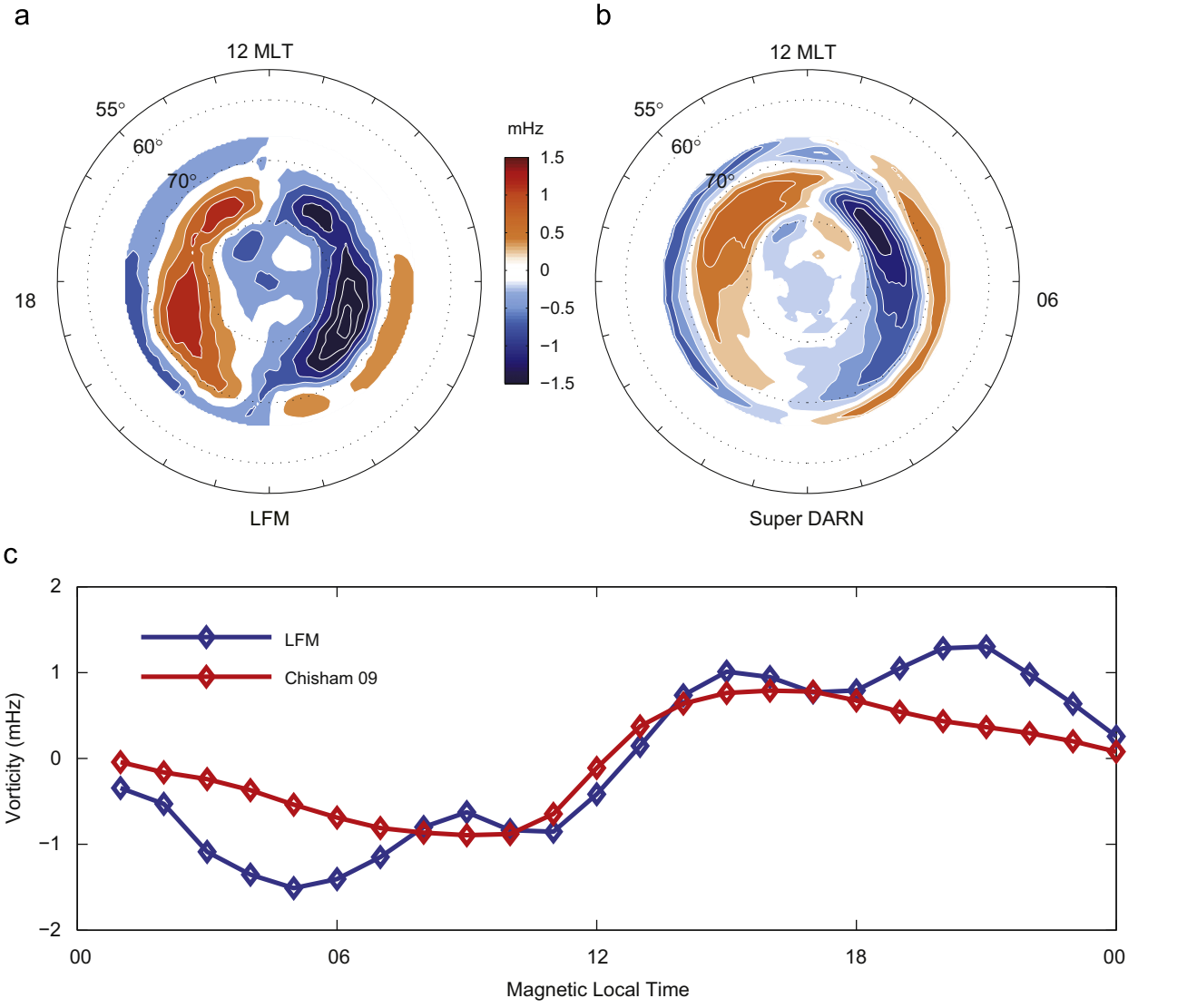

Fig. 10. Average distributions of ionospheric field-aligned vorticity obtained from (a) the LFM Long Run simulation and (b) six years of SuperDARN observation from Chisham et al. (2009). (c) Magnetic local time distributions of average vorticity between 72° and 77° latitude for both LFM simulation and SuperDARN observation.

inclusive) of SuperDARN line-of-sight velocity measurements, binned by IMF clock angles.

Fig. 10a and b shows the comparison of average ionospheric field-aligned vorticity derived from LFM simulation and SuperDARN measurements. Two main features are evident in the LFM average vorticity map. First, positive (negative) vorticity occurs at latitudes of 65°–70° in the morning (evening) sector. These features are approximately colocated with the Region II currents. Second, at higher latitudes of 70°–80° and overlapping the Region I currents, the average vorticity is negative in the morning sector and positive in the evening sector. The polar region ($>80°$ latitude) is weakly characterized by negative vorticity in the afternoon sector, which corresponds to the Region 0 currents. The statistical vorticity map derived from SuperDARN data also exhibits these features. Fig. 10c shows the magnetic local time distribution of average field-aligned vorticity between 72° and 77° latitude (the averaging interval used by Chisham et al., 2009) for both LFM simulation and SuperDARN measurements. The distributions show good agreement on the dayside. However, the average nightside vorticity in the LFM model is larger than that in the SuperDARN measurements. One possible reason for the deviation on the nightside is that in the LFM model, the ionospheric Pedersen conductance, determined by electron precipitation on the nightside, is relatively small, which gives high vorticity according to Eq. (8). On the other hand, extrapolation of SuperDARN measurements on the typically undersampled nightside may underestimate the ionospheric convection velocity there which would result in a smaller vorticity.

Fig. 11a shows the distributions of average vorticity calculated from the LFM simulation binned by IMF clock angle. Fig. 11b shows the average clock-angle binned vorticity map derived from SuperDARN measurements by Chisham et al. (2009). The LFM

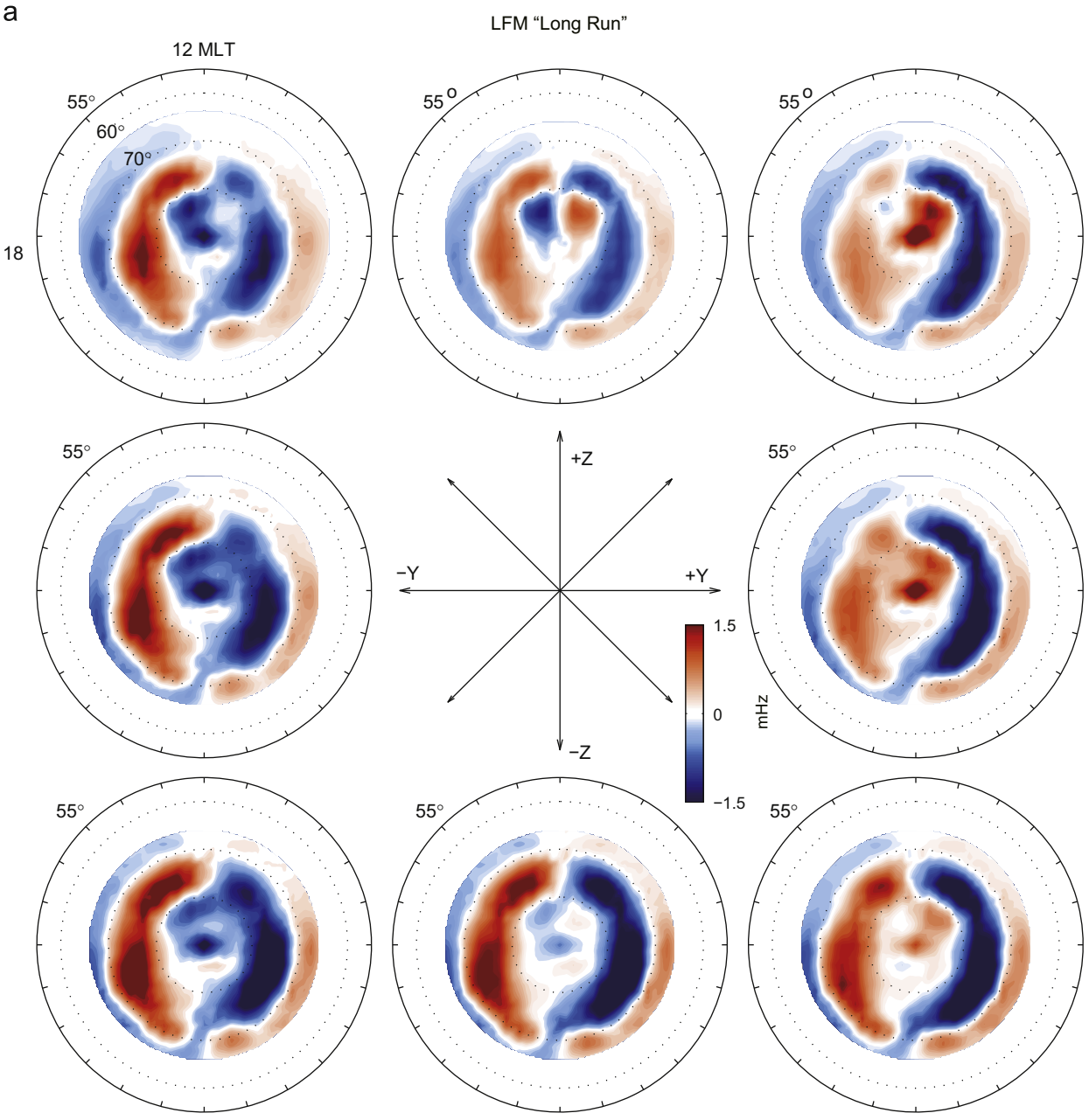

Fig. 11. Statistical distributions of ionospheric field-aligned vorticity obtained from (a) the LFM Long Run simulation and (b) SuperDARN observation from Chisham et al. (2009), binned by IMF clock angle.

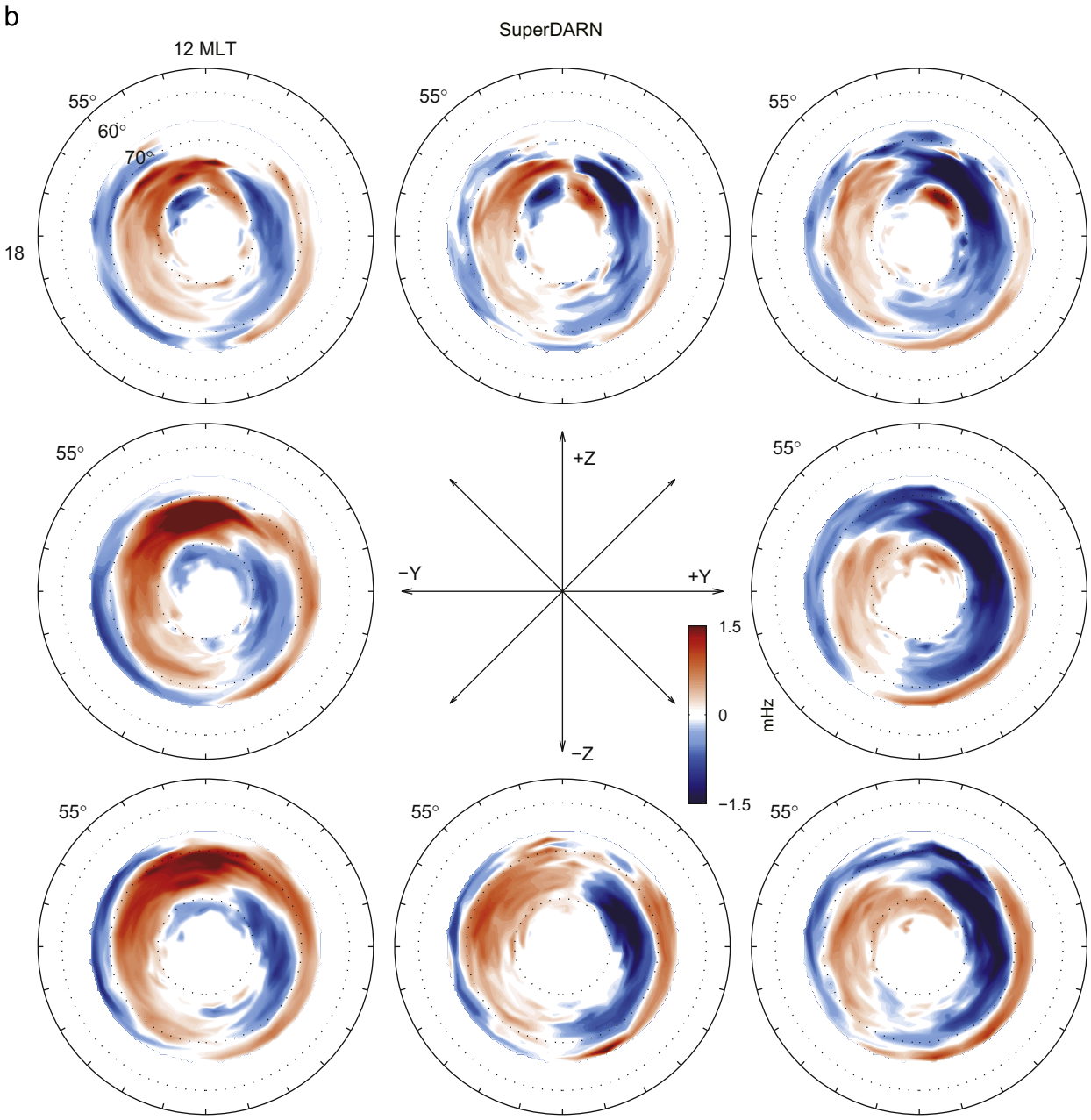

Fig. 11. (*Continued*)

model results exhibit systematic variations as the IMF clock angle rotates similar to those evident in the SuperDARN results. The topology and evolution of the global distributions of average vorticity are similar to those of the field-aligned current distributions shown in Fig. 6.

In both LFM and SuperDARN results, when IMF is northward ($B_z > 0$), the average vorticity is positive (negative) on the duskside (dawnside) in the high-latitude ionosphere between 70° and 80° where Region I currents flow. In the lower latitude ionosphere, between 65° and 70° where Region II currents flow, the average vorticity is negative (positive) on the duskside (dawnside). However, the latitudinal width of the vorticity distribution in the LFM simulation is broader than in SuperDARN results, especially for the lower latitude regions. In the polar region, inside 80° latitude, the average vorticity exhibits a two-component pattern similar to the NBZ current system. When the IMF clock angle rotates to 90° (270°), the topology of average vorticity pattern is preserved while the polar region is characterized by positive (negative) vorticity corresponding to the outward (inward) Region 0 currents. However, the LFM simulation does not have the wrap behavior near the noon region since the convection and field-aligned patterns are more symmetric. This is partially due to the lack of a corotating inner magnetosphere in the LFM simulation. When the IMF is southward ($B_z < 0$), the topology of average vorticity distribution is preserved and the intensity increases approximately by a factor of 2. The main difference between the LFM simulation results and SuperDARN measurements is that on the nightside, the average vorticity in the LFM model is greater for all IMF clock angle bins in the areas colocated with Region I currents. When IMF is southward, the deviation is maximum. The IMF conditions in the Long Run simulation are not likely to be precisely statistically similar to those for the SuperDARN results, which may explain some of this discrepancy. Even so, given that the nightside field-aligned currents are weaker in the Long Run than observed, this large deviation

implies that the nightside ionospheric conductance is too small in the LFM model. Therefore, in the regions where Region I currents flow, the average vorticity is higher in the simulation.

4. Summary and conclusions

We have presented a statistical data-model comparison of MI coupling using the archived LFM Long Run simulation data from the Guild et al. (2008a) study. Results show that in the LFM model, the average current systems consist of the familiar Region I and Region II current systems of Iijima and Potemra (1976a). The ionospheric Region II currents in the MHD simulation originate from the diamagnetic ring current. The dependence of the average field-aligned distributions on IMF clock angle in the LFM simulation is similar to that of both the Iridium global current distributions and the Weimer 05 empirical model. However, the magnitude of the average ionospheric field-aligned currents in the simulation is smaller than both observational and empirical results.

The statistical dependence of high-latitude convection patterns on IMF clock angle is similar to that of both the SuperDARN measurements and the empirical results from the Weimer 05 model. However, the average CPCP from the LFM model is greater than SuperDARN observational results approximately by a factor of 2, and is greater than Weimer 05 empirical results approximately by a factor of 1.5. The average convection patterns in the LFM simulation are more symmetric while both the SuperDARN data and the Weimer model have a significant dawn–dusk asymmetry.

Comparison of average Poynting flux patterns shows that in the LFM model, more Poynting flux flows into the polar region ionosphere while in the Weimer 05 model, most of the Poynting flux flows at lower latitudes in the ionosphere where Region I currents close with Region II currents. Therefore, in the LFM model, most of the dawnside Region I currents close to the duskside Region I currents through the polar region. This feature of the simulation model is a consequence of the higher CPCP in the LFM simulation, which allows higher electric field in the polar region.

Distributions of average ionospheric field-aligned vorticity derived from the LFM simulation are also compared with a statistical model based on SuperDARN measurements. The comparison of results exhibits good agreement on the dayside ionosphere. However, on the nightside ionosphere, the average vorticity from the LFM model is greater than the SuperDARN measurements. Given that the nightside currents in the Long Run simulation are weaker than observed, this result implies that the Pedersen conductance on the nightside ionosphere is too small in the LFM model. Therefore, a better ionospheric conductance model, or, alternatively, a better electron precipitation model, may significantly improve the fidelity of the LFM global simulations. In the LFM model, since the ionospheric conductance is regulated by the electron precipitation model, either new physical processes must be introduced in the precipitation model or empirical parameters in the model may need adjustment.

Acknowledgments

The research was supported by the NASA Sun-Earth Connection Theory Program (Grant # NNX08AI36G), the NASA Living With a Star Targeted Research and Technology Program (Grant # NNX07AQ16G) and the Center for Integrated Space Weather Modeling funded by the NSF STC program under cooperative agreement ATM-0120950. This research was also supported by the National Center for Atmospheric Research, which is sponsored by the National Science Foundation. Computing resources for the research were provided by the National Center for Atmospheric Research under CISL Project # 36761008.

B. Zhang and W. Lotko would also like to acknowledge the hospitality and support of the UCAR Advanced Study Program during summer 2009 when portions of the research were completed.

References

Anderson, B.J., Korth, H., Waters, C.L., Green, D.L., Stauning, P., 2008. Statistical Birkeland current distribution from the magnetic field observations by the Iridium constellation. Ann. Geophys. 26, 671–687.

Chisham, G., Freeman, M.P., Abel, G.A., Bristow, W.A., Marchaudon, A., Rouhoniemi, J.M., Sofko, G.J., 2009. The spatial distribution of average vorticity in the high latitude ionosphere and its variation with interplanetary magnetic field direction and season. J. Geophys. Res. 114, A09301. doi:10.1029/2009JA014263.

Fedder, J.A., Slinker, S.P., Lyon, J.G., Elphinstone, R.D., 1995. Global numerical simulation of the growth phase and the expansion onset for substorm observed by Viking. J. Geophys. Res. 85, 664.

Green, D.L., Waters, C.L., Anderson, B.J., Korth, H., 2009. Seasonal and interplanetary magnetic field dependence of the field-aligned currents for both northern and southern hemisphere. Ann. Geophys. 27, 1701–1715.

Guild, T.B., Spence, H.E., Kepko, E.L., Merkin, V., Lyon, J.G., Wiltberger, M., Goodrich, C.C., 2008a. Geotail and LFM comparisons of plasma sheet climatology: 1. Average values. J. Geophys. Res. 113, A04216. doi:10.1029/2007JA012611.

Guild, T.B., Spence, H.E., Kepko, E.L., Merkin, V., Lyon, J.G., Wiltberger, M., Goodrich, C.C., 2008b. Geotail and LFM comparisons of plasma sheet climatology: 2. Flow variability. J. Geophys. Res. 113, A04217. doi:10.1029/2007JA012613.

Iijima, T., Potemra, T.A., 1976a. The amplitude distribution of field-aligned currents at northern high latitudes observed by Triad. J. Geophys. Res. 81, 2165.

Iijima, T., Potemra, T.A., 1976b. Field-aligned currents in the dayside cusp observed by Triad. J. Geophys. Res. 81, 5971–5979.

Iijima, T., Potemra, T.A., Zanetti, L.J., Bythrow, P.F., 1984. Large-scale Birkeland currents in the dayside polar region during strongly northward IMF: a new Birkeland current system. J. Geophys. Res. 89, 7441–7452.

Janhunen, P.H., Koskinen, E.J., Pulkkinen, I.I., 1996. A new global ionosphere-magnetosphere coupling simulation utilizing locally varying time step. In: Proceedings of Third International Conference on Substorms (ICS 3), Versailles, France, May 12–17, Eur. Space Agency Spec. Publ., ESA SP-389, pp. 205–210.

Lotko, W., 2007. The magnetosphere–ionosphere system from the perspective of plasma circulation: a tutorial. J. Atmos. Sol. Terr. Phys. 69 (3), 191–211.

Lyon, J.G., Fedder, J.A., Mobarry, C.M., 2004. The Lyon–Fedder–Mobarry (LFM) global MHD magnetospheric simulation code. J. Atmos. Sol. Terr. Phys. 66 (1333.23), 648–650.

Pettigrew, E.D., Shepherd, S.G., Ruohoniemi, J.M., in press. Climatological patterns of high-latitude convection in the northern and southern hemispheres: dipole tilt dependencies and interhemispheric comparisons. J. Geophys. Res.

Raeder, J., 2003. Global geospace modeling: tutorial and review. In: Buchner, C., Dum, T., Scholer, M. (Eds.), Space plasma simulation, Lecture Notes in Physics, vol. 615. Springer-Verlag, pp. 212–246.

Robinson, R.M., Vondrak, R.R., Miller, K., Babbs, T., Hardy, D.A., 1987. On calculating ionospheric conductivities from the flux and energy of precipitating electrons. J. Geophys. Res. 92, 2565.

Slinker, S.P., Fedder, J.A., Emery, B.A., Baker, K.B., Lummerzheim, D., Lyon, J.G., Rich, F.J., 1999. Comparison of global MHD simulations with AMIE simulations for the events of May 19–20, 1996. J. Geophys. Res. 104, 28,379.

Sofko, G.J., Greenwald, R.A., Bristow, W., 1995. Direct determination of large-scale magnetospheric field-aligned currents with SuperDARN. Geophys. Res. Lett. 22, 2041–2044.

Weimer, D.R., 2005. Improved ionospheric electrodynamic models and application to calculating Joule heating rates. J. Geophys. Res. 110, A05306. doi:10.1029/2004JA010884.

Wiltberger, M., Wang, W., Burns, A.G., Solomon, S.C., Lyon, J.G., Goodrich, C.C., 2004. Initial results from the coupled magnetosphere ionosphere thermosphere model: magnetospheric and ionospheric responses. J. Atmos. Sol. Terr. Phys. 66 (15–16) Towards an Integrated Model of the Space Weather System, October–November 2004, pp. 1411–1423, ISSN 1364-6826, DOI:10.1016/j.jastp.2004.03.026..

Wiltberger, M., Weigel, R.S., Lotko, W., Fedder, J.A., 2009. Modeling seasonal variations of auroral particle precipitation in a global-scale magnetosphere–ionosphere simulation. J. Geophys. Res. 114, A01204.

Wolf, R.A., Spiro, R.W., Sazykin, S., Toffoletto, F.R., 2007. How the Earth's inner magnetosphere works: an evolving picture. J. Atmos. Sol. Terr. Phys. 69, 288–302.